Neodymium isotope constraints on chemical weathering and past glacial activity in Svalbard

Kwangchul Jang[a], Germain Bayon[b], Yeongcheol Han[a], Young Ji Joo[a], Ji-Hoon Kim[c], Jong-Sik Ryu[d], Jusun Woo[e], Matthias Forwick[f], Witold Szczuciński[g], Jung-Hyun Kim[a], and Seung-Il Nam[a,*]

[a]Division of Polar Paleoenvironment, Korea Polar Research Institute, Incheon 21990, South Korea

[b]IFREMER, Marine Geosciences Unit F-29280 Plouzané, France

[c]Petroleum and Marine Resources Research Division, Korea Institute of Geoscience and Mineral Resources, Daejeon 34132, South Korea

[d]Department of Earth and Environmental Sciences, Pukyong National University, Busan 48513, South Korea

[e]School of Earth and Environmental Sciences, Seoul National University, Seoul 08826, South Korea

[f]UiT The Arctic University of Norway, Department of Geosciences, NO-9037 Tromsø, Norway

[g]Geohazards Lab, Institute of Geology, Adam Mickiewicz University in Poznań, 61-680 Poznań, Poland

Submitted to *Earth and Planetary Science Letters*, September 2019

Revision submitted, April 2020

*Corresponding author. Tel.: +82-32-760-5362; Fax: +82-32-760-5397; E-mail: sinam@kopri.re.kr

Abstract

Neodymium (Nd) isotopes in leached authigenic components of marine sediments have been increasingly used as a tracer of past ocean-water masses. Despite the general assumption that the Nd isotopic composition of solutes released during chemical weathering fingerprints the source rocks on continents, preferential dissolution of easily dissolvable phases may result in significant deviations in Nd isotopic composition between the solutes and the source rocks, with potential implications for the utility of Nd isotopes in paleoenvironmental studies. Here, we present the Nd isotopic compositions of leached and detrital fractions separated from bedrock and marine sediment samples from the Svalbard archipelago. Our goal is to further understand the behaviour of Nd isotopes during chemical weathering in glacial catchments and evaluate how glacier fluctuations and associated weathering congruency may have affected the export of dissolved Nd isotope signatures to seawater.

Our results confirm that terrestrial weathering on Svalbard causes considerable Nd isotopic decoupling between the leached and detrital fractions of fjord sediments ($\triangle\varepsilon_{Nd}$), resulting from the preferential dissolution of marine precipitates in glaciated catchments dominated by sedimentary rocks. We also show that the degree of Nd isotopic decoupling has fluctuated in response to climate variability on Svalbard during the Holocene, which is also as suggested by the occurrence of generally higher $\triangle\varepsilon_{Nd}$ values during periods of glacier advances in sediment cores retrieved from two different fjords (Dicksonfjorden and Woodfjorden). We posit that the high $\triangle\varepsilon_{Nd}$ values can be ascribed to incongruent chemical weathering of fresh rock flour produced by glacial abrasion. This finding suggests that the degree of Nd isotopic decoupling could be used as a new proxy for tracing glacial fluctuations and associated glacier-derived nutrient inputs to the marine realm.

Keywords: Neodymium isotopes, isotopic decoupling, incongruent weathering, glacier fluctuation, Svalbard

1. Introduction

Global warming is having a profound impact on marine and terrestrial environments, and its effects are particularly evident in polar regions, where glacier and sea-ice melting in combination with associated changes in surface albedo and ocean heat distribution are key mechanisms underlying polar amplification (Taylor et al., 2013 and references therein). Glacier melting and accompanying glacial rock weathering have been recently identified as an important source of nanoparticulate nutrients available for primary production in the ocean (Hawkings et al., 2015; Wadham et al., 2019), and they potentially play an important role in marine biogeochemical cycles (review in Wadham et al., 2019). However, the impact of glacier melting on nutrient releases and marine productivity relies on sparse datasets (Hawkings et al., 2015). One important requirement for further evaluations of the future relationship among climate changes, glacial weathering (understood as chemical weathering in glacial catchments), glacier melting, and marine ecosystems is the reconstruction of past responses of glaciers to climate and subsequent changes in meltwater discharge.

Neodymium (Nd) isotopes (often expressed using the ε_{Nd} notation) are widely used for reconstructing past changes in ocean circulation and continental weathering fluxes (e.g., Bayon et al., 2002; Jang et al., 2017; Rutberg et al., 2000). A general consensus on the use of Nd isotopes in paleoenvironmental studies is that negligible decoupling occurs during continental weathering and sedimentary processes. However, in recent decades, multiple studies from river systems have shown that preferential dissolution of labile phases relative to more resistant minerals during weathering leads to markedly different Nd isotopic signatures in dissolved and solid loads (Goldstein and Jacobsen, 1987), especially in sub-Arctic regions and glacier-covered areas (Andersson et al., 2001; Hindshaw et al., 2018a; Süfke et al., 2019). This evidence for decoupling of Nd isotopes in the glacial environment suggests that past episodes of glacial retreats and advances could have possibly affected the ε_{Nd} signatures of the dissolved loads exported to the ocean over centennial to millennial time scales in high-latitude regions (Hindshaw et al., 2018a). For instance, an increased supply of fresh rock substrates by glacial abrasion could have led to enhanced incongruent weathering on continents (Vance et al., 2009), which would have resulted in greater Nd isotopic decoupling during past cold

events because of the intrinsic Nd isotopic differences in rock-forming minerals. The importance of Nd isotopes in provenance studies and their utility for tracing past meltwater releases call for a better understanding of their behaviour during glacial weathering and further evaluation of how past glacial dynamics may have influenced the isotopic composition of dissolved Nd exported to the ocean.

In this study, we present an extensive set of Nd isotopic compositions measured in both labile and detrital fractions of a series of sedimentary and metamorphic rock samples and surface sediment samples from across the Svalbard archipelago. Our aim is to characterize the effect of incongruent silicate weathering on Nd isotopes. Two marine sediment cores from fjords covering the Holocene period were also analyzed to assess the impact of past glacial advances and retreats on Nd isotopic decoupling and the preservation of ε_{Nd} signatures by surrounding water masses. The Svalbard archipelago is largely covered by glaciers and has diverse bedrock compositions, including sedimentary, metamorphic and volcanic rocks (Dallmann and Elvevold, 2015). Thus, the area is well suited for investigating the behaviour of Nd isotopes during glacial weathering.

2. Background

2.1. Nd isotope behaviour during weathering

Easily dissolvable components in rocks and sediments, such as marine precipitates (e.g., bio-skeletal carbonates, phosphates and Fe-Mn oxides) and labile detrital minerals (e.g., volcanic components and accessory minerals) (Goldstein and Jacobsen, 1987; Hindshaw et al., 2018a), can be selectively extracted using chemical leaching methods (Bayon et al., 2002; Gutjahr et al., 2007). The comparison of radiogenic isotopic compositions between 'leachable' and residual silicate phases indicates whether isotopic decoupling may occur during continental weathering (e.g., Dausmann et al., 2019). A recent experimental investigation of Nd isotopes conducted on Svalbard (Dryadbreen and Fardalen river basins; Fig. 1) clearly showed that bedrock leachates and river waters presented more radiogenic Nd isotopic values (= higher ε_{Nd}) than the parent bedrocks (Hindshaw et al., 2018a), suggesting that the isotopic composition of dissolved Nd is controlled by the preferential dissolution of labile phases during weathering. While such decoupling is mostly observed in sedimentary

105 catchments (Goldstein and Jacobsen, 1987), where radiogenic labile components typically occur as
106 marine precipitates (e.g., Hindshaw et al., 2018a), preferential dissolution of easily dissolvable
107 accessory minerals such as apatite or titanite, can also result in decoupling in granitic catchments
108 (e.g., Dausmann et al., 2019; Süfke et al., 2019).

109 On continents, the extent or magnitude of incongruent weathering is considered to be
110 climate-dependent (Vance et al., 2009). Enhanced incongruent weathering of glacially eroded rock
111 substrates is generally thought to have occurred during past cold periods, and they most likely resulted
112 in an intensified release of radiogenic Nd and Pb isotopes into dissolved river loads and the marine
113 environment. This process has been inferred in part on the basis of pronounced radiogenic Pb isotope
114 excursions in various late Quaternary sediment records of dispersed Fe-Mn oxyhydroxide phases from
115 the North Atlantic (Gutjahr et al., 2009) and high Alpine lake sediments (Süfke et al., 2019).
116 Furthermore, Süfke et al. (2019) documented a trend towards more radiogenic authigenic Nd isotopic
117 values in an Alpine lake sediment record, suggesting that Nd isotopes could also record enhanced
118 incongruent weathering of glacially derived material in the past. Similarly, long-term variations in Pb
119 and Nd isotopes in North Atlantic ferromanganese crusts across the onset of Northern Hemisphere
120 glaciations have also been attributed to changes from chemical- to physical-dominated weathering
121 regimes on surrounding continents (Gutjahr et al., 2009; von Blanckenburg and Nägler, 2001).
122
123 *2.2. Study area*

124 This study is based on bedrock samples from multiple onshore locations as well as sediment
125 samples from various fjords on Spitsbergen, the largest island of the Svalbard archipelago (Fig. 1).
126 The Svalbard archipelago is located between approximately 74-81˚N and 10-35˚E and surrounded by
127 the Barents Sea and the Greenland Sea (Fig. 1). Three main water masses contribute to the
128 hydrography of Spitsbergen fjords: (1) relatively warm and saline Atlantic Water (AW; $T > 3.0$ and $S > 34.65$; Cottier et al., 2005 and references therein) carried by the West Spitsbergen Current (WSC;
130 Fig. 1), (2) cold and relatively fresh Arctic water (ArW; $-1.5 < T < 1$ and $34.3 < S < 34.8$; Cottier et
131 al., 2005 and references therein) by the Sørkapp Current, an extension of the East Spitsbergen Current

(ESC; Fig. 1), and (3) glacial meltwater (Cottier et al., 2005). Their mixing varies depending on location within a fjord, water depth, and season of a year, resulting in complex hydrography containing various water masses such as Surface Water (SW), Local Water (LW), Intermediate Water (IW), Transformed Atlantic Water (TAW), and Winter Cooled Water (WCW) (e.g., Promińska et al., 2017; Zajączkowski et al., 2010). A top-most layer in late spring and summer is occupied by fresh SW ($S < 34.00$), which is strongly affected by glacial meltwater. LW ($34.30 < S < 34.85$, $-0.5 < T < 1.0$) and WCW ($T < -0.5$, $34.40 < S < 35.00$) are formed by surface cooling during autumn and brine formation during winter, respectively, while TAW ($1.0 < T < 3.0$, $34.65 < S$) and IW ($34.00 < S < 34.65$, $T > 1.0$) are formed by mixing between AW and ArW, as well as various fjord masses (Cottier et al., 2005).

The bedrock geology of Svalbard in general as well as in the catchment areas of the studied fjords, is very diverse and ranges from Proterozoic metamorphic rocks to Phanerozoic sedimentary rocks (Dallmann and Elvevold, 2015) (Fig. 2). Hornsund is dominated by Proterozoic metamorphic rocks at the fjord mouth in the west to Palaeogene sedimentary rocks at the fjord head in the east. They display complicated structures, including folds, faults, and overthrusts (Dallmann and Elvevold, 2015). Similarly, the Van Mijenfjorden and Isfjorden systems display the longitudinal (W-E) variability in bedrock geology from Proterozoic metamorphic rocks to Carboniferous to Palaeogene sedimentary rocks. The catchment area of Dicksonfjorden, a northern tributary of Isfjorden, is composed of sedimentary sequences, including Devonian Old Red Sandstones and siltstones and Carboniferous-Permian carbonate-siliciclastic strata. The catchment area of Woodfjorden primarily consists of the Devonian Old Red Sandstone with a minor Quaternary volcanic complex, and Mesoproterozoic metamorphic and igneous rocks located at the heads of its tributaries (Fig. 2). The catchment of Wijdefjorden is dominated by Proterozoic to lower Silurian metamorphic rocks along the eastern shore and Upper Silurian to Devonian sedimentary rocks in the west (Dallmann and Elvevold, 2015).

During the Holocene, Svalbard experienced several phases of glacier advances and retreats. The deglaciation of the inner fjords of west Spitsbergen terminated approximately 11.2 ka (Baeten et

159 al., 2010; Forwick and Vorren, 2009), and a warming period in western Spitsbergen lasted until 9 to 8
160 ka (Forwick and Vorren, 2009; Rasmussen et al., 2012). Gradual cooling accentuated by several
161 asynchronous cooling steps (e.g., Rasmussen et al., 2012) followed this period (Forwick and Vorren,
162 2009). In particular, the enhanced growth and/or reformation of glaciers (Fjeldskaar et al., 2018), such
163 as Linnébreen, Nordenskiöldbreen, Tunabreen and those in the Hajeren lake catchment occurred
164 between 6 and 4 ka (Baeten et al., 2010; Forwick et al., 2010; Svendsen and Mangerud, 1997; van der
165 Bilt et al., 2015). Most glaciers reached their maximum Holocene extents during the Little Ice Age
166 (LIA) (~66 % with a total area of 38,871 km^2; Martín-Moreno et al., 2017). Glaciers have been
167 retreating since the termination of the LIA, and approximately 57% of Svalbard is currently covered
168 with glaciers (total area of 33,775 km^2; Martín-Moreno et al., 2017 and references therein).
169 The study focuses in particular on the analysis of two sediment cores from Dicksonfjorden
170 and Woodfjorden. The sediment supply to Dicksonfjorden occurs mainly by glacio-fluvial runoff. On
171 the other hand, the main sediment sources in Woodfjorden are glacio-fluvial rivers in inner
172 Woodfjorden and Bockfjorden as well as tidewater glaciers in Liefdefjorden. At present, WCW forms
173 by convection during the fall and winter seasons in both fjords. However, considering the known past
174 climate and glacier variations in Svalbard during the Holocene (Baeten et al., 2010; Rasmussen et al.,
175 2012; Svendsen and Mangerud, 1997), the oceanographic and sedimentary regime were different in
176 the past. The relative sea level fell by up to 65 m on Spitsbergen during the last 12 ka (Forman et al.,
177 2004). The most pronounced changes occurred at the end and shortly after the deglaciation, and only
178 minor changes have occurred since the middle Holocene.
179

180 **3. Materials and methods**

181 *3.1. Materials*

182 *3.1.1.* Bedrock

183 A total of 18 fresh unweathered rock samples from representative bedrock units of Svalbard
184 were collected (Isfjorden, n = 10; Kongsfjorden, n = 7; Woodfjorden, n = 1; Table 1 and Fig. 2).
185 Metamorphic rocks (i.e., quartzite and phyllite) were collected from the upper Proterozoic

Generalfjella Formation in the Kongsfjorden area, while sandstone samples were collected from Isfjorden, Billefjorden and Woodfjorden. The Woodfjorden sandstone corresponds to the Devonian Old Red Sandstone, which represents the main source of sediments in Dicksonfjorden and inner Woodfjorden. Carboniferous bedrock samples from the Kongsfjorden and Isfjorden areas are mainly composed of calcareous sedimentary rocks (limestone and dolostone), while the Mesozoic bedrock samples from Isfjorden include siliciclastic mudstones, siltstones, and sandstones.

3.1.2. Surface sediments

A total of 45 surface (0-1 cm sediment depth) and sub-surface sediment samples (up to 5-6 cm sediment depth) (hereafter, surface sediments) from Bockfjorden (n = 1), Dicksonfjorden (n = 8), Hornsund (n = 21), Liefjefjorden (n = 1), Tempelfjorden (n = 1), Van Mijenfjorden (n = 2), Wijdefjorden (n = 8) and Woodfjorden (n = 2) (Fig. 3) were collected to characterize the modern distribution of sedimentary Nd isotopes in Spitsbergen fjords. The material was retrieved with a giant box corer (50 × 50 × 50 cm^3) or a gravity corer during cruises of the *RV Helmer Hanssen* of UiT The Arctic University of Norway in 2012, 2015, 2016, and 2017 (Supplementary Table S1). The sampling sites are located at water depths ranging from 37 to 322 m, and they are in contact with the water masses mentioned earlier (*section 2.2*) depending on the fjord location, water depth and distance from the fjord mouth (e.g., Promińska et al., 2017; Zajączkowski et al., 2010).

3.1.3. Core sediments

Two gravity cores from Dicksonfjorden (HH16-1202-GC; 78.727˚N, 15.310˚E, ~87 m water depth) and Woodfjorden (HH12-964-GC; 79.651˚N, 13.755˚E, ~173 m water depth) were retrieved to reconstruct the evolution of sedimentary Nd isotopic compositions during the Holocene. Core HH16-1202-GC is ~274 cm long and spans the last 8.2 ka (Joo et al., 2019), with an average sediment accumulation rate of ~33 cm/ka. The lithology is dominated by reddish-brown mud that includes varying amounts of sandy detrital clasts. Core HH12-964-GC is ~334 cm long and spans the last ~13.3 ka (Hansen, 2014). The average sediment accumulation rate is 25.1 cm/ka, although rates of up

to 91 cm/ka were calculated for the lower parts of the core. The lithology of core HH12-964-GC is dominated by silt-sized sediment, with the occurrence of coarser intervals at ~110 cm and near the bottom of the core (Hansen, 2014). In each core, 1 cm thick sediment layers were collected at 10 cm intervals for the Nd isotope analyses (n = 28 for HH16-1202-GC and n = 35 for HH12-964-GC).

3.2. Analytical methods

3.2.1. Sample preparation

In this study, we define 'authigenic' and 'weatherable' components as the easily dissolvable fractions (e.g., carbonate, and Fe-Mn oxyhydroxide) extracted by chemical leaching from unwashed ground bulk sediments and from bedrock, respectively (Bayon et al., 2002; Gutjahr et al., 2007; Jang et al., 2017; Rutberg et al., 2000; Werner et al., 2014). The protocol used for chemical leaching is based on the addition of 0.02 M hydroxylamine hydrochloride in 25% acetic acid buffered to pH ~4 using NH_4OH (hereafter, HH solution) for less than 1 hour (Jang et al., 2017). The reagent-to-sample volume ratio was approximately 1 (Jang et al., 2017) to prevent the dissolution of labile detrital components (e.g., volcanic material) during the leaching process. Following the extraction of the authigenic and/or weatherable components, a second leaching step was carried out using the HH solution for ~24 hours to eliminate any remaining carbonate or Fe-Mn oxyhydroxide materials from the residual 'detrital' fraction (Jang et al., 2017).

After rinsing with Milli-Q water (Millipore, >18.2 MΩ cm), the detrital fractions were digested by alkaline fusion for Nd isotopic measurements (Bayon et al., 2009). Approximately 100 mg of dry ground detrital sediment was transferred into a glassy carbon beaker (SIGRADUR GAB 3, HTW) with 1.2 g of Na_2O_2 (>95%, small beads, ACS grade, Sigma-Aldrich) and 0.6 g of NaOH (>98.0%, pellet, ACS grade, Sigma-Aldrich) and placed in a furnace at ~700°C for ~15 min. Neodymium and other reactive elements were then co-precipitated onto Fe oxide phases after the addition of ultrapure Milli-Q water. After centrifugation, Fe oxide precipitates were rinsed in Milli-Q water and dissolved in 2 M HNO_3. Neodymium was purified by ion chromatography following a protocol modified from Pin and Zalduegui (1997) (Jang et al., 2017).

240

241 *3.2.2.* Elemental concentration analysis

242 The elemental abundances (Al, K, Ca, Mg, Fe, and rare earth elements (REEs)) of whole-
243 rock samples and detrital fractions were determined by inductively coupled plasma optical emission
244 spectrometry (ICP-OES, OPTIMA 8300, PerkinElmer) and mass spectrometry (ICP-MS, Thermo X-
245 5, Thermo Scientific) at the Korea Basic Science Institute (KBSI). Prior to the elemental analyses, the
246 samples were dissolved by acid digestion in a PTFA digestion vessel using a 4:4:1 mixture of HNO_3,
247 HF, and $HClO_4$. Repeated analyses of USGS rock reference powders (BCR-2 and BHVO-2) yielded a
248 reproducibility better than ±5% (1σ, standard deviation).

249

250 *3.2.3.* Nd isotope analyses

251 Neodymium isotopic measurements were performed by thermal ionization mass
252 spectrometry (TIMS, Triton, Thermo Scientific) at the Korea Polar Research Institute. All measured
253 ratios were corrected for mass fractionation using $^{146}Nd/^{144}Nd = 0.7219$. Repeated analyses of JNdi-1
254 standard solutions yielded an average value of $^{143}Nd/^{144}Nd = 0.512100 \pm 0.000011$ (2σ, n = 30), which
255 were consistent with the reference value (0.512115) of Tanaka et al. (2000). The validity of the
256 analytical procedure was further evaluated by analyzing the USGS reference materials BCR-2
257 (0.512631 ± 0.000013, 2σ, n = 3) and BHVO-1 (0.512975 ± 0.000009, 2σ, n = 3), which were also
258 consistent with values from the literature (e.g., Raczek et al., 2003). The total procedure blank was
259 < 0.2% Nd for the detrital fractions and an order of magnitude less for the leached authigenic phases.
260 In this study, Nd isotopic ratios are reported using the epsilon notation (ε_{Nd}), which represents the
261 deviation of any measured $^{143}Nd/^{144}Nd$ ratio relative to the value for the modern chondritic uniform
262 reservoir ($(^{143}Nd/^{144}Nd)_{CHUR} = 0.512638$; Jacobsen and Wasserburg, 1980).

263

264 **4. Results**

265 *4.1. Svalbard bedrocks*

266 Elemental and isotopic data for the detrital and weatherable fractions of the bedrock samples

(n = 18) are reported in Supplementary Table S2, Table 1, and Fig. 2. The Nd concentrations in these samples vary from ~0.3 to ~43 mg/kg for the bulk samples and from ~0.03 to ~33 mg/kg for the detrital components. Limestone, dolostone, and anhydrite are characterized by much lower Nd concentrations (0.3 to 4.0 mg/kg for bulk samples) compared with those in the siliceous sedimentary rocks, such as the Devonian Old Red Sandstone and the Permian black mudstone (up to ~43 mg/kg for bulk and ~35 mg/kg for the detrital component).

The detrital and weatherable fractions of the bedrocks display wide ranges of ε_{Nd} values, from -25.9 to 3.4 and from -25.6 to -1.2, respectively (Fig. 2). The average values of detrital and weatherable ε_{Nd} are -9.8 ± 6.6 (1σ, n = 14) and -9.8 ± 5.7 (1σ, n = 15), respectively, and the two isotopic compositions are strongly correlated with each other (r = 0.82, n = 14). The Cretaceous sandstone and the mid-Jurassic to early Cretaceous shale collected close to the mouth of Isfjorden presented the minimum ε_{Nd} value (-25.9 for detrital and -25.6 for weatherable) and maximum ε_{Nd} value (+3.4 for detrital and -1.2 for weatherable) measured in the bedrocks. Note that analyses of Nd-poor bedrocks, such as anhydrite (< 0.4 mg/kg for bulk), limestone (< 4 mg/kg for bulk) and two dolostone samples (< 1.3 mg/kg for bulk), were not possible due to insufficient intensity signals during the TIMS analysis. Except for the Cretaceous sandstone and the upper Proterozoic phyllite, the Nd isotopic compositions of the weatherable fractions are statistically different from the corresponding detrital fractions. Except for three Mesozoic shales, the weatherable ε_{Nd} signatures are systematically more radiogenic (up to 5 epsilon-units higher) than the corresponding detrital fractions (Figs. 3 & 4).

4.2. Fjord surface sediments

The Nd concentrations of the bulk samples and their detrital components of the surface sediments show average values of 48 and 40 mg/kg, respectively. Thus, they are higher than the maximum concentrations reported for the bedrock samples (see *section 4.1*). The ε_{Nd} compositions of the detrital components range from -24.9 to -10.1 (with an average of -14.7 ± 3.0; 1σ, n = 45), while those of the authigenic components are more radiogenic, ranging from -14.5 to -9.0 (with an average

of -11.5 ± 1.5; 1σ, n = 45) (Figs. 3 & 4). The correlation between the detrital and authigenic ε_{Nd} is strong (r = 0.62) but not as strong as that of the bedrock. Note that the sediments collected from Hornsund, with average detrital and authigenic ε_{Nd} values of -15.1 ± 3.0 and -10.8 ± 1.5 (1σ, n = 21), respectively, display a large spatial variability reflecting the presence of various bedrock types in the surrounding catchment area, including Proterozoic metamorphic rocks and Palaeozoic, Mesozoic and Palaeogene sedimentary sequences (Dallmann and Elvevold, 2015). The sediments recovered from Dicksonfjorden are comparatively uniform in terms of Nd isotopes, with average detrital and authigenic ε_{Nd} values of -13.6 ± 0.1 and -11.5 ± 0.2 (1σ, n = 8), respectively, which are very similar to the composition of the Devonian Old Red Sandstone (-13.6 ± 0.3 and -10.8 ± 0.2, respectively). Similar detrital ε_{Nd} values were also obtained for sediments from Woodfjorden and its tributary fjords (-13.6 ± 0.5, 1σ, n = 4). However, the elemental ratios (e.g., Fe/Ca and Ca/Al; Supplementary Table S3) and sediment colours are different from that in Dicksonfjorden. In Wijdefjorden, the detrital ε_{Nd} values of surface sediments are between those of the Devonian Old Red Sandstone (-13.6 ± 0.3) collected from the Woodfjorden catchments (Fig. 2B) and Paleoproterozoic meta-igneous rocks from Ny-Friesland (ε_{Nd} ~ -25.4 to -18.6 from Johansson et al., 1995) (Fig. 2A). The sediments collected in Van Mijenfjorden are characterized by less radiogenic detrital ε_{Nd} values of -17.3 and -16.9.

4.3. Core sediments

4.3.1. Dicksonfjorden

Sediments at site HH16-1202 in Dicksonfjorden are characterized by detrital and authigenic ε_{Nd} values ranging from -14.5 to -12.9 (average -13.5 ± 0.3, 1σ, n = 28), and from -11.5 to -10.4 (average -11.2 ± 0.2), respectively (Fig. 5). Compared with the bedrock and core-top sediment samples, the detrital and authigenic ε_{Nd} values at site HH16-1202 display only a moderate correlation over the past 7.6 ka (r = 0.43, n = 28). Some ε_{Nd} excursions can be detected in the core for both detrital and authigenic fractions (e.g., the more radiogenic value at ~3.5 ka) as well as only for the detrital (less radiogenic ε_{Nd} shifts during the last millennia) or authigenic fractions (e.g., more radiogenic authigenic value at ~4.5 ka).

321

322 *4.3.2.* Woodfjorden

323 The detrital ε_{Nd} values at site HH12-964 in Woodfjorden fluctuated from -14.5 to -8.7 over
324 the last 13.3 ka (Fig. 6), whereas the authigenic fractions displayed a much narrower range of ε_{Nd}
325 signatures (from -11.8 to -10.6; average value -11.2 ± 0.3, 1σ, n = 35) (Fig. 6). For the detrital
326 fractions, the average ε_{Nd} value of -13.4 is consistent with that of the Devonian Old Red Sandstone.
327 Prominent peaks in the detrital ε_{Nd} values towards radiogenic signatures occurred at ~7.2 ka and ~13.2
328 ka. The overall downcore trend of authigenic values ε_{Nd} does not correlate with that of the detrital ε_{Nd}
329 values (r = -0.07), which is probably due to several outliers in the detrital ε_{Nd} trend.

330

331 **5. Discussion**

332 *5.1. Nd isotopic decoupling during incongruent terrestrial weathering in Svalbard*

333 The weatherable components extracted from the analyzed bedrocks usually display more
334 radiogenic Nd isotopic compositions than the corresponding detrital silicate fractions (Figs. 3 & 4).
335 Enriched radiogenic Nd isotope ratios of leachates could be found, such as in volcanogenic sediments
336 (e.g., Elmore et al., 2011). However, we are confident that the observed radiogenic Nd isotopic
337 composition in the weatherable fraction does not result from the preferential dissolution of labile
338 volcanic components due to four reasons (Supplementary Text 1). First, our mild leaching procedure
339 would have prevented any significant detrital contamination (Jang et al., 2017). Second, if significant
340 detrital contamination had occurred, then preferential leaching of the volcanogenic sediment in core
341 HH12-964 should have occurred, which would have yielded pronounced radiogenic signatures in the
342 leached authigenic fractions (which is not the case). Third, the authigenic ε_{Nd} signature at site HH17-
343 1086 in Wijdefjorden (Fig. 1) is statistically consistent with the neighbouring seawater ε_{Nd} (see more
344 detail in *section* 5.2.1). Finally, although the sediments collected from two proximal sites in Hornsund
345 display similar detrital ε_{Nd} and major element geochemistry, they present different authigenic ε_{Nd}
346 values, which is consistent with their overlying bottom water masses showing contrasting water
347 temperatures (see more detail in *section* 5.2.2).

As a consequence, the observed Nd isotopic decoupling between the weatherable and detrital components of Svalbard bedrocks is most likely best explained by the preferential dissolution of marine precipitates hosted by sedimentary rocks and/or labile accessory mineral phases in silicate rocks. The same hypothesis was recently proposed by Hindshaw et al. (2018a) to account for the observation that dissolved riverine loads in Svalbard were more radiogenic than corresponding suspended sediments, bedrocks, and glacial sediments (Fig. 4). In full agreement with this finding, our rock leaching experiments demonstrate that incongruent weathering in Svalbard can lead to significant Nd isotopic decoupling (Supplementary Text 2). Sedimentary rocks consist of various biogenic and authigenic components that are generally admixed with older recycled detrital minerals derived from the erosion of the basement and presumably characterized by less radiogenic ε_{Nd} compositions (e.g., Hindshaw et al., 2018b).

Previous studies have also reported pronounced Nd isotopic differences between dissolved loads and suspended sediments or bedrocks in catchments (Andersson et al., 2001; Goldstein and Jacobsen, 1987), particularly in sub-arctic river systems draining old metamorphic rocks (Andersson et al., 2001). Preferential alteration of easily dissolvable and radiogenic accessory minerals, such as apatite or titanite, is likely to occur during the weathering of igneous and metamorphic rocks (e.g., Andersson et al., 2001; von Blanckenburg and Nägler, 2001) as demonstrated by the rock leaching experiments (Dausmann et al., 2019).

In this study, significant Nd isotopic decoupling between detrital and weatherable fractions (> 1.2 epsilon-units) was observed in one of the two metamorphic rock samples and 11 of the 12 sedimentary rock samples, with the most pronounced isotopic decoupling (about 9 epsilon-units) occurring in the Carboniferous sandstone (Figs. 3 & 4). Interestingly, the ε_{Nd} differences between the weatherable and detrital fractions in sedimentary rocks were not always positive and presented negative values in four samples (Figs. 3 & 4). This finding contradicts the common assumption that incongruent weathering leads to the release of more radiogenic Nd fractions compared to residual detrital fractions (Andersson et al., 2001; Dausmann et al., 2019; Goldstein and Jacobsen, 1987; Hindshaw et al., 2018a; von Blanckenburg and Nägler, 2001). The negative ε_{Nd} offsets were found in

375 the Carboniferous sandstone (with a Nd isotopic difference of -9 epsilon-units) and three Mesozoic
376 shale samples (with ε_{Nd} differences between -3.0 and -4.6 epsilon-units); thus, in these samples, the
377 detrital ε_{Nd} values are comparatively more radiogenic than the weatherable ε_{Nd} values. The presence of
378 abundant radiogenic mineral phases, such as zircon or garnet (characterized by high Sm/Nd ratios; see
379 Fig. 2 in Bayon et al., 2006), in silicate residual phases could account for the observed ε_{Nd} differences
380 between the weatherable and detrital fractions. However, it is also likely that these negative ε_{Nd}
381 differences reflect the fact that detrital fractions in sedimentary rocks may have been derived from the
382 erosion of silicate bedrocks that are more radiogenic than associated weatherable marine precipitates.
383
384 *5.2. Origin of the authigenic ε_{Nd} in Svalbard fjord sediments*
385 *5.2.1.* Terrestrial signals
386 The strong Nd isotope correlation (r = 0.62) observed between authigenic and detrital
387 fractions of Svalbard fjord sediments suggests that the ε_{Nd} signature of leached phases is mainly
388 influenced by terrestrial inputs (Fig. 4). As reported previously, the presence of preformed Fe oxides
389 delivered together with detrital inputs could at least partially account for these 'terrestrial' ε_{Nd}
390 signatures (Bayon et al., 2004; Werner et al., 2014). Such preformed terrestrial Fe oxides can be
391 entrained in sea-ice (Werner et al., 2014) or delivered via riverine inputs (Bayon et al., 2004).
392 However, preformed Fe oxides do not account for the characteristic features of authigenic ε_{Nd}
393 described in *section 5.2.2*.
394 Alternatively, glacial meltwater runoff to the fjords through glacial rivers or direct outflows
395 from tidewater glaciers is known to deliver substantial amounts of dissolved and nanoparticulate iron
396 (Poulton and Raiswell, 2005; Wadham et al., 2019; Wehrmann et al., 2014), and this is also the case
397 for Svalbard, where large inputs of dissolved iron and Fe oxides can occur as a result of the glacial
398 abrasion and subsequent dissolution of silicate rocks or iron-bearing sedimentary rocks (Hindshaw et
399 al., 2018a; Wehrmann et al., 2014). This mechanism can be further promoted in polar regions by the
400 photoreductive dissolution of Fe oxides trapped in ice (Kim et al., 2010). In Svalbard, this process
401 may be linked to markedly higher contents of highly reactive Fe oxides observed in fine-grained

glacial meltwater sediments in Finsterwalderbreen compared to other glacial and riverine sediments in the world (Poulton and Raiswell, 2005). Iron oxide in such sediments is mainly hosted by clay-bound nanoparticulate Fe oxides (10-20 nm diameter) (Poulton and Raiswell, 2005), which can be easily dissolved in seawater (Moore et al., 1979), hence representing a potential source of dissolved iron (and presumably REEs) for subsequent authigenic Fe-oxyhydroxide co-precipitation in Svalbard fjords.

Vertical benthic fluxes related to the early diagenetic iron cycle in marine sediments represent another substantial source of dissolved iron in Svalbard fjords. The diagenetic reduction of glacially derived Fe oxides and the subsequent release of dissolved iron into pore waters may enhance the *in-situ* formation of authigenic minerals in near-surface sediments, e.g., monosulphides and siderite (Görlich, 1986). This process is revealed by the high dissolved Fe concentrations (up to 800 μM) determined in porewaters in Kongsfjorden and Van Keulenfjorden (Wehrmann et al., 2014) and other evidence for intense early diagenetic Fe reductions in other Svalbard fjords (e.g., Hornsund, Tempelfjorden and Van Mijenfjorden; Vandieken et al., 2006 and references therein). The reduction of Fe oxide releases abundant REEs. Therefore, the high export fluxes of dissolved Fe to Svalbard fjords are also accompanied by the delivery of substantial amounts of dissolved REEs.

5.2.2. Seawater signals

One seawater ε_{Nd} data point is available from North Svalbard Sta#2 ($\varepsilon_{Nd} \sim -11.8 \pm 0.4$ from Andersson et al., 2008; 78.834˚N, 9.330˚E, ~199 m water depth) located only approximately 22 km north-north west from the core site HH17-1086 (top-core authigenic $\varepsilon_{Nd} \sim -11.4 \pm 0.3$), i.e., the northernmost station of Wijdefjorden (Fig. 1). The two sites lie at water depths of 150 m and 322 m in comparable water masses characterized by the same density. The ε_{Nd} values of seawater and authigenic sediment at both sites are consistent within uncertainty, suggesting the authigenic ε_{Nd} as an archive of seawater Nd isotopic signatures (not preformed Fe oxides).

The seawater signals recorded in the authigenic ε_{Nd} can also be evaluated by comparing the results from two nearby sites in Hornsund; HH15-1472 and HH16-1230 (for locations see Table S2

and Fig. 3). These two sites are located less than 2.2 km from each other but are separated by a sill and hence are affected by different water masses, namely, TAW (HH15-1472) and WCW (HH16-1230) (Promińska et al., 2017; Zajączkowski et al., 2010) (Fig. 3). The ambient bottom water masses at both sites can be clearly distinguished by different summer season temperatures, which are approximately 1°C in the outer fjord basin (TAW) and below -1°C in the inner basin (WCW) (Zajączkowski et al., 2010). The surface sediments collected at the two sites show the same detrital ε_{Nd} values and almost identical major elemental geochemical composition, such as K/Al, Ca/Al, Fe/Ca and Mg/Al ratios (Supplementary Table S3). However, the samples display different authigenic ε_{Nd} values (-12.1 at site HH15-1472 and -9.6 at site HH16-1230). This observation further highlights that the authigenic ε_{Nd} signal preserved in the surface fjord sediments in Svalbard could be derived, at least to some extent, from local water masses.

The authigenic ε_{Nd} values of the surface sediments collected near glacier fronts in Hornsund (i.e., sampling sites HH16-1230, HH15-1482, and HH15-1486) are much more radiogenic than those of the regionally advected water mass within the Sørkapp Current, which is an extension of the ESC ($-11.6 < \varepsilon_{Nd} < -10.6$ from Laukert et al., 2017; station 13; 78.834˚N, 9.330˚E, ~199 m water depth) (Fig. 1), suggesting strong preservation of radiogenic terrestrial inputs near the sources. Strong terrestrial signals could be partly due to efficient flocculation and, thus, the capture of small particles (including Fe oxides) and their rapid deposition in the proximal environment (Markussen et al., 2016). However, limitations exist in the simple comparison of isotopic compositions. Due to the transformation of water masses carried by ESC and mixing with Atlantic water masses within WSC on the continental shelf of western Spitsbergen, the water masses entering Hornsund fjord are a mixture of various water masses (e.g., Promińska et al., 2017). Therefore, we cannot rule out the influence of seawater inflow on the radiogenic authigenic ε_{Nd}.

5.3. Variation in the degree of Nd isotopic decoupling linked to climate-driven glacial system changes

In Svalbard fjords, the authigenic ε_{Nd} values measured in surface sediments are

systematically more radiogenic than the corresponding detrital ε_{Nd} signatures. Consistent with previous experimental investigations (see *section 5.1*), this observation further suggests that the preferential release of radiogenic Nd occurs during weathering in a glacial environment.

Similar observations can be drawn from the downcore records acquired from Dicksonfjorden (site HH16-1202; Supplementary Table S4) and Woodfjorden (site HH12-964; Supplementary Table S5), where the authigenic ε_{Nd} values are typically more radiogenic than the detrital ε_{Nd} values (Figs. 5 & 6). Interestingly, the differences between the authigenic and detrital values ($\triangle\varepsilon_{Nd}$) at these two sites display similar variability over time (Fig. 7). Neodymium isotopic decoupling was enhanced (i.e., leading to more positive $\triangle\varepsilon_{Nd}$ values) since the mid-Holocene, when new glaciers formed (Fjeldskaar et al., 2018; Svendsen and Mangerud, 1997; van der Bilt et al., 2015) (growth curve of valley glacier in Fig. 7) and/or existing glaciers on Svalbard readvanced ~4.5 ka (Baeten et al., 2010; Forwick et al., 2010) (growth curve of ice cap in Fig. 7). Decoupling is even more markedly enhanced during the transition period and main phase of LIA, when most glaciers on Svalbard reached their maximum extent (e.g., Martín-Moreno et al., 2017; Svendsen and Mangerud, 1997) (Fig. 7).

Based on the above discussion (*section 5.2*), the observed strong decoupling between authigenic and detrital signatures during the colder periods could indicate increasing contribution from (1) less radiogenic detrital materials, (2) inflow of radiogenic seawater and/or (3) more labile terrestrial sources in the glaciated catchments. The first hypothesis, although it could partly explain maximum $\triangle\varepsilon_{Nd}$ values at the onset of and during parts of the LIA (Figs 5, 6, and 7) when decreased ε_{Nd} of detrital fractions were documented, cannot account for the significant change in the $\triangle\varepsilon_{Nd}$ value during the period of glacier growth at ~4.5 ka. Unfortunately, the very high diversity of rock types on Svalbard combined with the sparse dataset on the measured ε_{Nd} in rocks (Table 1) limits the ability to provide an exact explanation (sediment sources) for the observed temporal variability of ε_{Nd} in the studied sediment cores. The second hypothesis concerning the enhanced inflow of advected seawater likely cannot explain the observed changes, at least in Dicksonfjorden because of a shallow (~20 m) sill at the fjord mouth, which has become slightly shallower in response to an isostatic rebound during the mid-Holocene (Forman et al., 2004), thereby further restricting the inflow of external water

masses. The third hypothesis concerning the increased input of labile terrestrial materials seems to provide a good explanation of the changes, particularly those recorded in Dicksonfjorden, where the increased sediment accumulation rate ~4.5 ka (Fig. 5) indicates enhanced terrestrial inputs related to the glacio-fluvial processes at that time. The glacial activity in Dicksonfjorden likely increased at approximately 4.5 ka. This timing is synchronous with the glacier reformation in the catchment areas of Linnévatnet (5 - 4 ka from Svendsen and Mangerud, 1997) and Hajeren lakes (~4.3 and ~3.3 ka from van der Bilt et al., 2015) (Fig. 7). It also corresponded to the periods when Nordenskiöldbreen in Billefjorden (5.5 - 3.2 ka from Baeten et al., 2010) and Tunabreen in Tempelfjorden (6 - 4 ka from Forwick et al., 2010) grew (Fig. 7). Based on the evidence above, we propose that the downcore fluctuations in $\triangle\varepsilon_{Nd}$ in Svalbard fjord sediments, mainly at ~4.5 ka when several catchments were likely re-occupied by glaciers, reflected changes in the degree of ε_{Nd} decoupling related to the presence/growth (or absence/retreat) of adjacent glaciers and associated weathering conditions. We hypothesize that the growth of glaciers provided freshly eroded rock substrates available for subglacial weathering, thereby leading to the preferential release of radiogenic Nd (e.g., Süfke et al., 2019) and ultimately more pronounced isotopic decoupling between authigenic and detrital ε_{Nd} values in the fjord sediments (Fig. 7). An increase in the $\triangle\varepsilon_{Nd}$ value at site HH12-964 in mid-Woodfjorden at approximately 4.5 ka may also be attributed to the growth of tidewater glaciers draining into the Woodfjorden system (Fig. 7), which is supported by an abrupt increase in the sand content at that time (from less than 2 to 4.4 %; Hansen, 2014). We ruled out the potential influence of preformed Fe oxides based on the discussion in section 5.2. However, the presence of preformed phases within sediment that survived weak chemical weathering during the periods of glacier advances might partly intensify $\triangle\varepsilon_{Nd}$ by increasing the authigenic ε_{Nd}.

Our finding that $\triangle\varepsilon_{Nd}$ variability in Svalbard fjord sediments may reflect weathering-induced changes in Nd isotopic decoupling related to glacier cover has far-reaching implications. For instance, $\triangle\varepsilon_{Nd}$ could be used in future studies to reconstruct the impact of past glacial meltwater on marine productivity (e.g., Wadham et al., 2019) as a proxy to infer historical glacial releases of key nutrients (e.g., P and Fe) associated with the dissolution of accessory phosphate minerals and nano-particulate

510 iron oxides.

511

512 **6. Conclusion**

513 Our survey of Nd isotopes in leached and residual (detrital) components of Svalbard bedrock
514 and fjord sediment samples confirms that weathering under glacial conditions is accompanied by
515 incongruent weathering leading to significant Nd isotope decoupling. In Arctic environments, such as
516 Svalbard, glacier melting provides substantial amounts of nanoparticulate Fe oxides and dissolved
517 elements, resulting in abundant co-precipitation of hydrogenous Fe-oxyhydroxide phases in the
518 nearby seawater/fjord environments and controlling, to a large extent, the distribution of leached
519 authigenic ε_{Nd} values in fjord sediments. The difference between authigenic and detrital ε_{Nd} values
520 (termed $\triangle\varepsilon_{Nd}$) in the Holocene sedimentary records from the two fjords, Dicksonfjorden and
521 Woodfjorden show trends that mimic the evolution of glacier activity over the last millennia, related
522 to climate variability. The $\triangle\varepsilon_{Nd}$ values and inferred Nd isotopic decoupling were higher during the
523 periods of glacier advances, e.g., at ~4.5 ka and during the LIA, suggesting that increased glacier
524 cover and concomitant glacial abrasion of fresh rock substrates resulted in intensified incongruent
525 chemical weathering. This novel Nd isotope approach ($\triangle\varepsilon_{Nd}$) may be used in future studies as a new
526 proxy for past glacial changes and associated glacial-derived nutrient inputs to the marine realm.

527

528 **Acknowledgments**

529 This study was mainly supported by the Basic Core Technology Development Program for
530 the Oceans and the Polar Regions (NRF-2015M1A5A1037243), the Basic Science Research Program
531 (2017R1A6A3A01076729) from the NRF funded by MSIT, South Korea, and the National Science
532 Centre in Poland (2013/10/E/ST10/00166). We would like to thank S. D. Hur, C. Han and J. Baek for
533 helping with the instrumental analysis and D. Kim, K. Park, Y. Ahn, Y. Joe and Y. Son for laboratory
534 assistance. The captains and crews of R/V Helmer Hanssen supported the core sampling during the
535 cruise. Many thanks to two anonymous reviewers for numerous constructive suggestions for
536 improving the manuscript

537

538 **References**

539 Andersson, P.S., Dahlqvist, R., Ingri, J., Gustafsson, Ö., 2001. The isotopic composition of Nd in a
540 boreal river: a reflection of selective weathering and colloidal transport. Geochim. Cosmochim. Acta
541 65, 521-527.
542 Andersson, P.S., Porcelli, D., Frank, M., Björk, G., Dahlqvist, R., Gustafsson, Ö., 2008. Neodymium
543 isotopes in seawater from the Barents Sea and Fram Strait Arctic–Atlantic gateways. Geochim.
544 Cosmochim. Acta 72, 2854-2867.
545 Baeten, N.J., Forwick, M., Vogt, C., Vorren, T.O., 2010. Late Weichselian and Holocene sedimentary
546 environments and glacial activity in Billefjorden, Svalbard. Geol. Soc. Lond., Spec. Publ. 344, 207-223.
547 Bayon, G., Barrat, J.A., Etoubleau, J., Benoit, M., Bollinger, C., Révillon, S., 2009. Determination of
548 rare earth elements, Sc, Y, Zr, Ba, Hf and Th in geological samples by ICP-MS after Tm addition and
549 alkaline fusion. Geostand. Geoanal. Res. 33, 51-62.
550 Bayon, G., German, C.R., Boella, R.M., Milton, J.A., Taylor, R.N., Nesbitt, R.W., 2002. An improved
551 method for extracting marine sediment fractions and its application to Sr and Nd isotopic analysis.
552 Chem. Geol. 187, 179-199.
553 Bayon, G., German, C.R., Burton, K.W., Nesbitt, R.W., Rogers, N., 2004. Sedimentary Fe-Mn
554 oxyhydroxides as paleoceanographic archives and the role of aeolian flux in regulating oceanic
555 dissolved REE. Earth Planet. Sci. Lett. 224, 477-492.
556 Bayon, G., Vigier, N., Burton, K.W., Brenot, A., Carignan, J., Etoubleau, J., Chu, N.-C., 2006. The
557 control of weathering processes on riverine and seawater hafnium isotope ratios. Geology 34, 433-436.
558 Cottier, F., Tverberg, V., Inall, M., Svendsen, H., Nilsen, F., Griffiths, C., 2005. Water mass modification
559 in an Arctic fjord through cross-shelf exchange: The seasonal hydrography of Kongsfjorden, Svalbard.
560 J. Geophys. Res. Oceans 110.
561 Dallmann, W., Elvevold, S., 2015. Bedrock Geology. Geoscience Atlas of Svalbard, Norsk Polarinstitutt,
562 Tromsø, Report Series 148, 133-173.
563 Dausmann, V., Gutjahr, M., Frank, M., Kouzmanov, K., Schaltegger, U., 2019. Experimental evidence

564 for mineral-controlled release of radiogenic Nd, Hf and Pb isotopes from granitic rocks during
565 progressive chemical weathering. Chem. Geol. 507, 64-84.
566 Elmore, A., Piotrowski, A., Wright, J., Scrivner, A., 2011. Testing the extraction of past seawater Nd
567 isotopic composition from North Atlantic deep sea sediments and foraminifera. Geochem. Geophys.
568 Geosyst. 12, Q09008, https://doi .org /10 .1029 /2011GC003741.
569 Fjeldskaar, W., Bondevik, S., Amantov, A., 2018. Glaciers on Svalbard survived the Holocene thermal
570 optimum. Quat. Sci. Rev. 199, 18-29.
571 Forman, S., Lubinski, D., Ingólfsson, Ó., Zeeberg, J., Snyder, J., Siegert, M., Matishov, G., 2004. A
572 review of postglacial emergence on Svalbard, Franz Josef Land and Novaya Zemlya, northern Eurasia.
573 Quat. Sci. Rev. 23, 1391-1434.
574 Forwick, M., Vorren, T.O., 2009. Late Weichselian and Holocene sedimentary environments and ice
575 rafting in Isfjorden, Spitsbergen. Palaeogeogr. Palaeoclimatol. Palaeoecol. 280, 258-274.
576 Forwick, M., Vorren, T.O., Hald, M., Korsun, S., Roh, Y., Vogt, C., Yoo, K.-C., 2010. Spatial and
577 temporal influence of glaciers and rivers on the sedimentary environment in Sassenfjorden and
578 Tempelfjorden, Spitsbergen. Geol. Soc. Lond., Spec. Publ. 344, 163-193.
579 Goldstein, S.J., Jacobsen, S.B., 1987. The Nd and Sr isotopic systematics of river-water dissolved
580 material: Implications for the sources of Nd and Sr in seawater. Chem. Geol. 66, 245-272.
581 Görlich, K., 1986. Glacimarine sedimentation of muds in Hornsund fjord, Spitsbergen. Ann. Soc. Geol.
582 Pol. 56, 433-477.
583 Gutjahr, M., Frank, M., Halliday, A.N., Keigwin, L.D., 2009. Retreat of the Laurentide ice sheet tracked
584 by the isotopic composition of Pb in western North Atlantic seawater during termination 1. Earth Planet.
585 Sci. Lett. 286, 546-555.
586 Gutjahr, M., Frank, M., Stirling, C.H., Klemm, V., van de Flierdt, T., Halliday, A.N., 2007. Reliable
587 extraction of a deepwater trace metal isotope signal from Fe-Mn oxyhydroxide coatings of marine
588 sediments. Chem. Geol. 242, 351-370.
589 Hansen, T., 2014. Late Weichselian and Holocene sedimentary processes and glacier dynamics in
590 Woodfjorden, Bockfjorden and Liefdefjorden, North Spitsbergen. The Arctic University of Norway.

591 Hawkings, J., Wadham, J., Tranter, M., Lawson, E., Sole, A., Cowton, T., Tedstone, A., Bartholomew,
592 I., Nienow, P., Chandler, D., 2015. The effect of warming climate on nutrient and solute export from the
593 Greenland Ice Sheet. Geochem. Perspect. Lett 1, 94-104.
594 Hindshaw, R.S., Aciego, S.M., Piotrowski, A.M., Tipper, E.T., 2018a. Decoupling of dissolved and
595 bedrock neodymium isotopes during sedimentary cycling. Geochem. Perspect. Lett. 8, 43-46.
596 Hindshaw, R.S., Tosca, N.J., Piotrowski, A.M., Tipper, E.T., 2018b. Clay mineralogy, strontium and
597 neodymium isotope ratios in the sediments of two High Arctic catchments (Svalbard). Earth Surf.
598 Dynam. 6, 141-161.
599 Jacobsen, S.B., Wasserburg, G.J., 1980. Sm-Nd isotopic evolution of chondrites. Earth Planet. Sci. Lett.
600 50, 139-155.
601 Jang, K., Huh, Y., Han, Y., 2017. Authigenic Nd isotope record of North Pacific Intermediate Water
602 formation and boundary exchange on the Bering Slope. Quat. Sci. Rev. 156, 150-163.
603 Johansson, Å., Gee, D., Björklund, L., Witt-Nilsson, P., 1995. Isotope studies of granitoids from the
604 Bangenhuk formation, Ny Friesland Caledonides, Svalbard. Geol. Mag. 132, 303-320.
605 Joo, Y.J., Forwick, M., Park, K., Joe, Y., Son, Y.J., Nam, S.-I., 2019. Holocene environmental changes
606 in Dicksonfjorden, west Spitsbergen, Svalbard. Polar Res. 38, 3426, https://doi .org /10 .33265
607 /polar.v38 .3426.
608 Kim, K., Choi, W., Hoffmann, M.R., Yoon, H.-I., Park, B.-K., 2010. Photoreductive dissolution of iron
609 oxides trapped in ice and its environmental implications. Environ. Sci. Technol. 44, 4142-4148.
610 Laukert, G., Frank, M., Bauch, D., Hathorne, E.C., Rabe, B., von Appen, W.-J., Wegner, C., Zieringer,
611 M., Kassens, H., 2017. Ocean circulation and freshwater pathways in the Arctic Mediterranean based
612 on a combined Nd isotope, REE and oxygen isotope section across Fram Strait. Geochim. Cosmochim.
613 Acta 202, 285-309.
614 Markussen, T.N., Elberling, B., Winter, C., Andersen, T.J., 2016. Flocculated meltwater particles
615 control Arctic land-sea fluxes of labile iron. Sci. Rep.-UK 6, 24033, https://doi .org /10 .1038
616 /srep24033.
617 Martín-Moreno, R., Allende Álvarez, F., Hagen, J.O., 2017. 'Little Ice Age' glacier extent and

618 subsequent retreat in Svalbard archipelago. The Holocene 27, 1379-1390.
619 Moore, R., Burton, J., Williams, P.L., Young, M., 1979. The behaviour of dissolved organic material,
620 iron and manganese in estuarine mixing. Geochim. Cosmochim. Acta 43, 919-926.
621 Pin, C., Zalduegui, J.S., 1997. Sequential separation of light rare-earth elements, thorium and uranium
622 by miniaturized extraction chromatography: Application to isotopic analyses of silicate rocks. Anal.
623 Chim. Acta 339, 79-89.
624 Poulton, S.W., Raiswell, R., 2005. Chemical and physical characteristics of iron oxides in riverine and
625 glacial meltwater sediments. Chem. Geol. 218, 203-221.
626 Promińska, A., Cisek, M., Walczowski, W., 2017. Kongsfjorden and Hornsund hydrography –
627 comparative study based on a multiyear survey in fjords of west Spitsbergen. Oceanologia 59, 397-412.
628 Raczek, I., Jochum, K.P., Hofmann, A.W., 2003. Neodymium and strontium isotope data for USGS
629 reference materials BCR-1, BCR-2, BHVO-1, BHVO-2, AGV-1, AGV-2, GSP-1, GSP-2 and eight
630 MPI-DING reference glasses. Geostandard. Newslett. 27, 173-179.
631 Rasmussen, T.L., Forwick, M., Mackensen, A., 2012. Reconstruction of inflow of Atlantic Water to
632 Isfjorden, Svalbard during the Holocene: Correlation to climate and seasonality. Mar. Micropaleontol.
633 94, 80-90.
634 Rutberg, R.L., Hemming, S.R., Goldstein, S.L., 2000. Reduced North Atlantic Deep Water flux to the
635 glacial Southern Ocean inferred from neodymium isotope ratios. Nature 405, 935-938.
636 Süfke, F., Gutjahr, M., Gilli, A., Anselmetti, F.S., Glur, L., Eisenhauer, A., 2019. Early stage weathering
637 systematics of Pb and Nd isotopes derived from a high-Alpine Holocene lake sediment record. Chem.
638 Geol. 507, 42-53.
639 Svendsen, J.I., Mangerud, J., 1997. Holocene glacial and climatic variations on Spitsbergen, Svalbard.
640 The Holocene 7, 45-57.
641 Tanaka, T., Togashi, S., Kamioka, H., Amakawa, H., Kagami, H., Hamamoto, T., Yuhara, M., Orihashi,
642 Y., Yoneda, S., Shimizu, H., Kunimaru, T., Takahashi, K., Yanagi, T., Nakano, T., Fujimaki, H., Shinjo,
643 R., Asahara, Y., Tanimizu, M., Dragusanu, C., 2000. JNdi-1: a neodymium isotopic reference in
644 consistency with LaJolla neodymium. Chem. Geol. 168, 279-281.

645 Taylor, P.C., Cai, M., Hu, A., Meehl, J., Washington, W., Zhang, G.J., 2013. A decomposition of
646 feedback contributions to polar warming amplification. J. Climate 26, 7023-7043.
647 van der Bilt, W.G.M., Bakke, J., Vasskog, K., D'Andrea, W.J., Bradley, R.S., Ólafsdóttir, S., 2015.
648 Reconstruction of glacier variability from lake sediments reveals dynamic Holocene climate in Svalbard.
649 Quat. Sci. Rev. 126, 201-218.
650 Vance, D., Teagle, D.A., Foster, G.L., 2009. Variable Quaternary chemical weathering fluxes and
651 imbalances in marine geochemical budgets. Nature 458, 493-496.
652 Vandieken, V., Finke, N., Jørgensen, B.B., 2006. Pathways of carbon oxidation in an Arctic fjord
653 sediment (Svalbard) and isolation of psychrophilic and psychrotolerant Fe(III)-reducing bacteria. Mar.
654 Ecol. Prog. Ser. 322, 29-41.
655 von Blanckenburg, F., Nägler, T.F., 2001. Weathering versus circulation-controlled changes in
656 radiogenic isotope tracer composition of the Labrador Sea and North Atlantic Deep Water.
657 Paleoceanography 16, 424-434.
658 Wadham, J.L., Hawkings, J.R., Tarasov, L., Gregoire, L.J., Spencer, R.G.M., Gutjahr, M., Ridgwell, A.,
659 Kohfeld, K.E., 2019. Ice sheets matter for the global carbon cycle. Nat. Commun. 10, 3567.
660 Wehrmann, L.M., Formolo, M.J., Owens, J.D., Raiswell, R., Ferdelman, T.G., Riedinger, N., Lyons,
661 T.W., 2014. Iron and manganese speciation and cycling in glacially influenced high-latitude fjord
662 sediments (West Spitsbergen, Svalbard): Evidence for a benthic recycling-transport mechanism.
663 Geochim. Cosmochim. Acta 141, 628-655.
664 Werner, K., Frank, M., Teschner, C., Müller, J., Spielhagen, R.F., 2014. Neoglacial change in deep water
665 exchange and increase of sea-ice transport through eastern Fram Strait: evidence from radiogenic
666 isotopes. Quat. Sci. Rev. 92, 190-207.
667 Zajączkowski, M., Szczuciński, W., Plessen, B., Jernas, P., 2010. Benthic foraminifera in Hornsund,
668 Svalbard: Implications for paleoenvironmental reconstructions. Pol. Polar Res. 31, 349-375.

669

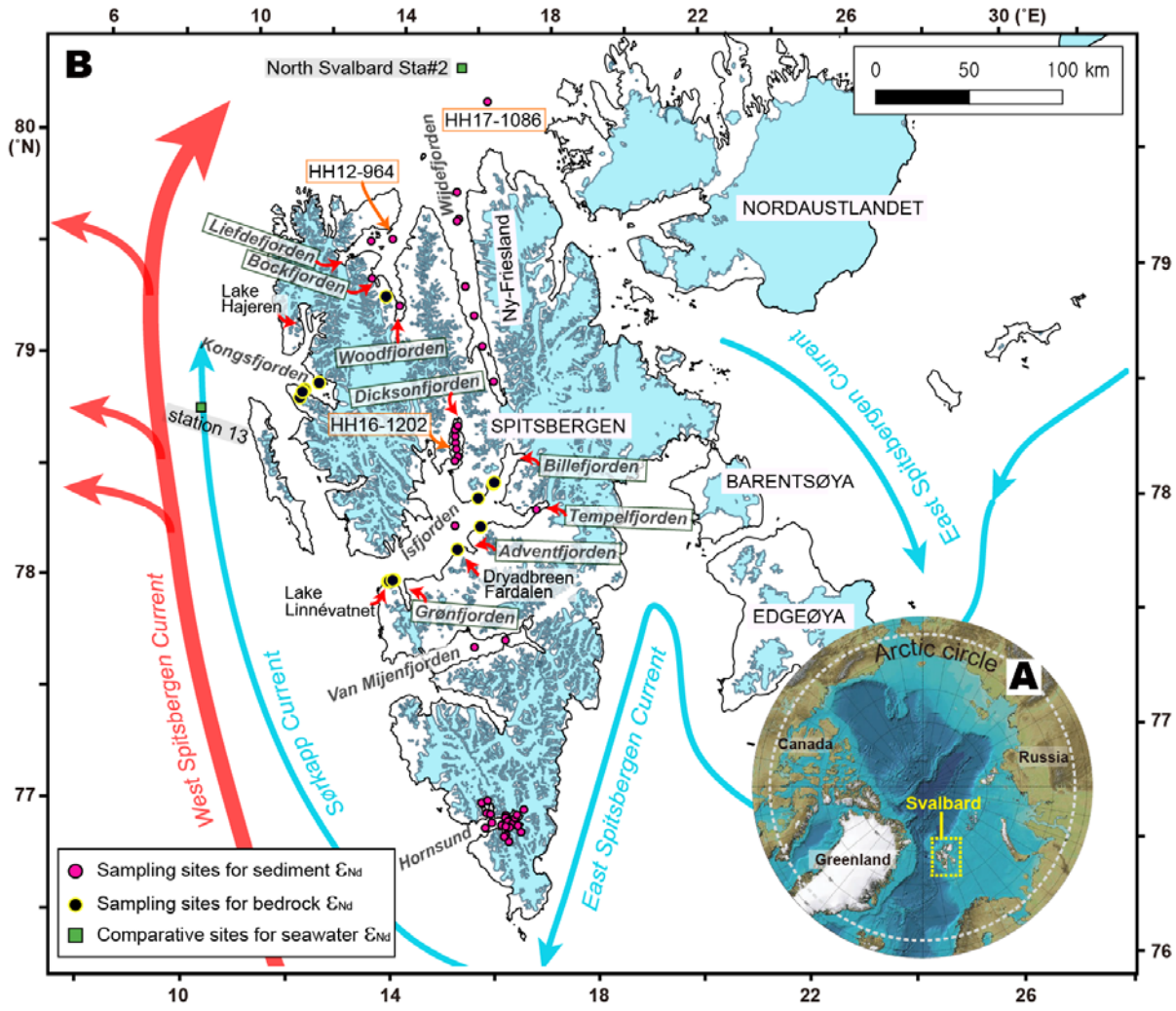

Figure 1. (A) Map of the Arctic showing the location of the Svalbard archipelago. (B) Map of the Svalbard archipelago. Locations of bedrock and fjord-sediments sample as well as place names mentioned in the text are indicated. Sky blue land areas represent the glacier coverage at present. Red and sky blue arrows indicate the West Spitsbergen Current (WSC) and the Sørkapp Current (branch of the East Spitsbergen Current (ESC)), respectively. The comparative sites (North Svalbard Sta#2 and station 13) for the ε_{Nd} values of Atlantic Water and Arctic Water inflows carried by the WSC and the ESC, respectively, are also shown. See Table S1 for the coordinates of the sampling and comparative sites.

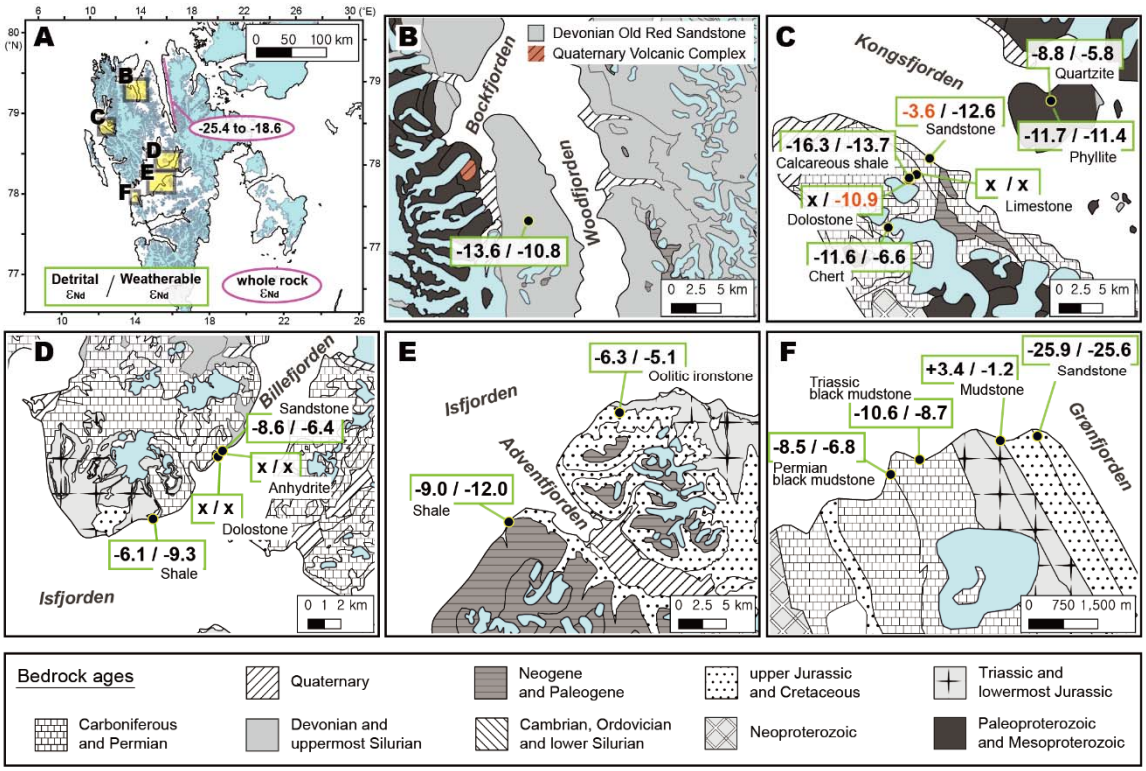

Figure 2. (A) Map of Svalbard showing the sampling locations (B) to (F) for the bedrock. The ε_{Nd} values of detrital and weatherable components in the catchment areas of Woodfjorden (B), Kongsfjorden (C) and Isfjorden and its tributary Billefjorden (D, E, and F) are marked with green rectangles. Samples with too little Nd to obtain data are marked with an 'x'. ε_{Nd} values with high uncertainties (> 0.5 epsilon-unit) are in red numbers. The bedrock samples include sixteen sedimentary rocks and two metamorphic rocks. Various bedrock ages are marked with different symbols. For comparison, the ε_{Nd} value measured from whole rocks in Ny-Friesland (for location see Fig. 1) is also marked with pink ellipses in Fig 2A (data from Johansson et al., 1995). The geologic map is modified after Dallmann and Elvevold (2015).

693

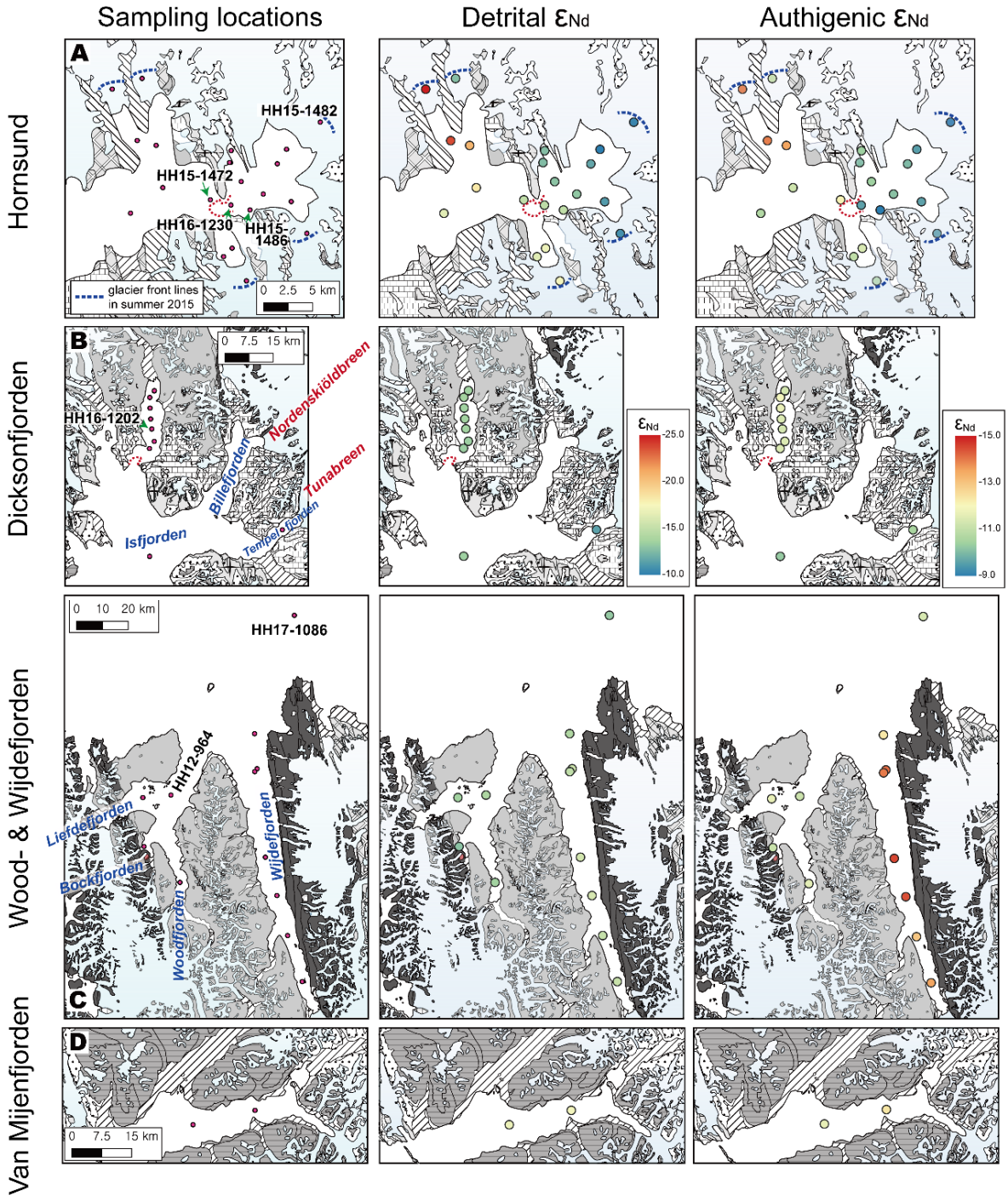

694

695 **Figure 3.** Maps of the locations of fjord sediments (left column). ε_{Nd} of detrital (central column) and
696 authigenic (right column) components within surface sediments collected from (A) Hornsund,
697 (B) Dicksonfjorden, Isfjorden, Tempelfjorden, (C) Woodfjorden, Wijdefjorden, and (D) Van
698 Mijenfjorden. The present glacier fronts in Hornsund (summer 2015) are indicated by blue
699 dashed lines, and major sills in Hornsund and Dicksonfjorden are marked by red dotted lines.

700

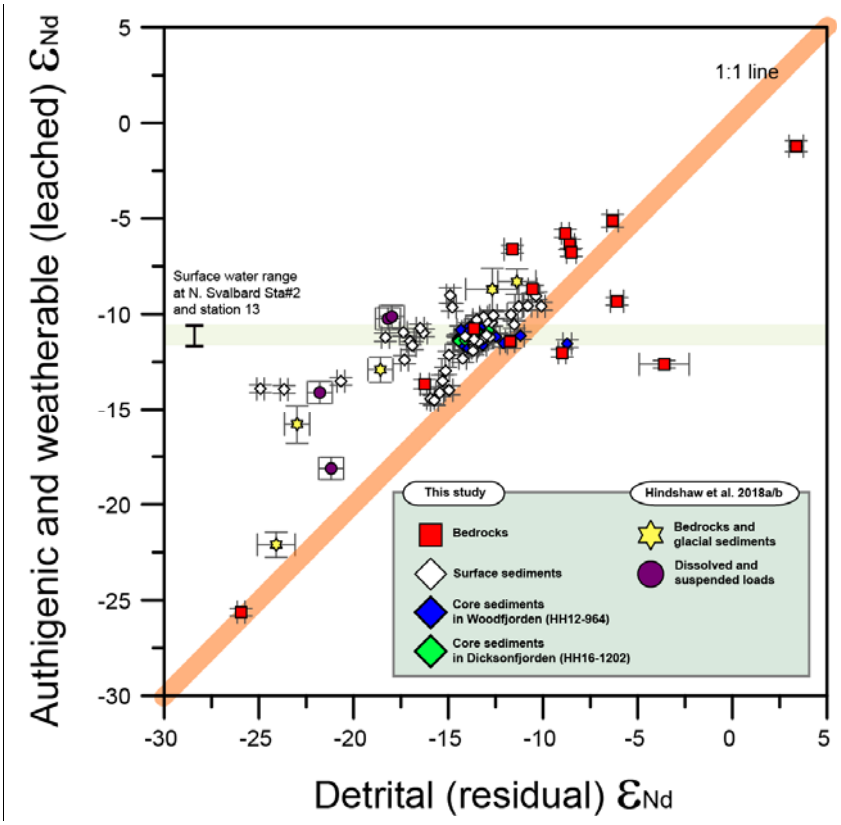

Figure 4. ε_{Nd} data comparison between leached (authigenic and weatherable) and residual components (detrital) of the bedrock samples (red squares), surface sediments (white diamonds), core sediments at sites HH12-964 (blue diamonds) and HH16-1202 (green diamonds). For further comparison, the ε_{Nd} values of the corresponding components within bedrocks and glacial sediments (yellow stars) and riverine dissolved and suspended loads (purple circles) in Svalbard, as well as seawater range at the Spitsbergen margin (green bar) are also shown (data from Andersson et al., 2008; Hindshaw et al., 2018a; Hindshaw et al., 2018b; Laukert et al., 2017).

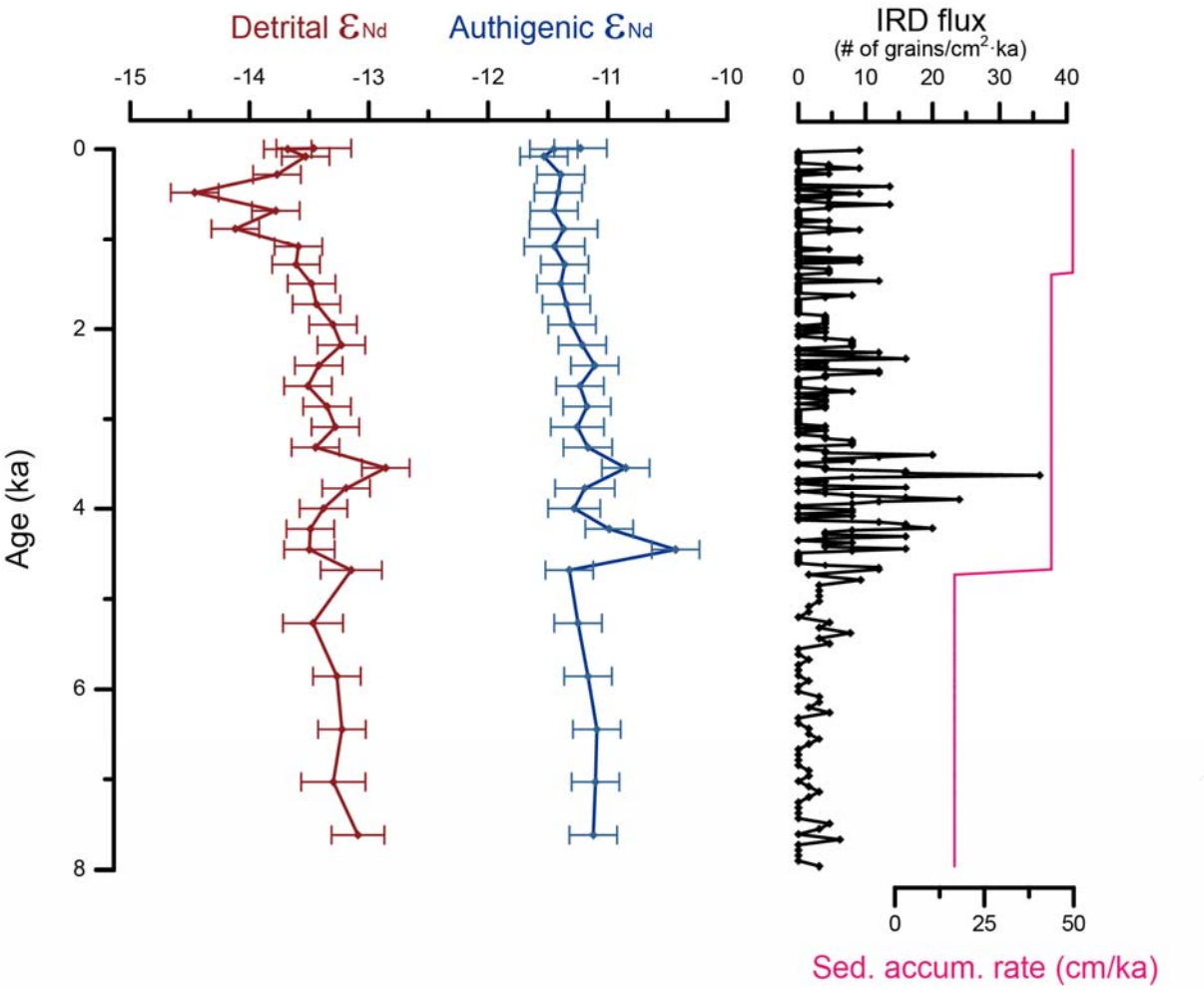

711

712 **Figure 5.** Temporal variation in ε_{Nd} values of detrital (red) and authigenic (blue) components at site
713 HH16-1202 in Dicksonfjorden. The ε_{Nd} data are compared to the IRD flux (black) and sediment
714 accumulation rate (dark pink) (Joo et al., 2019). Error bars for ε_{Nd} represent ±2σ uncertainties.

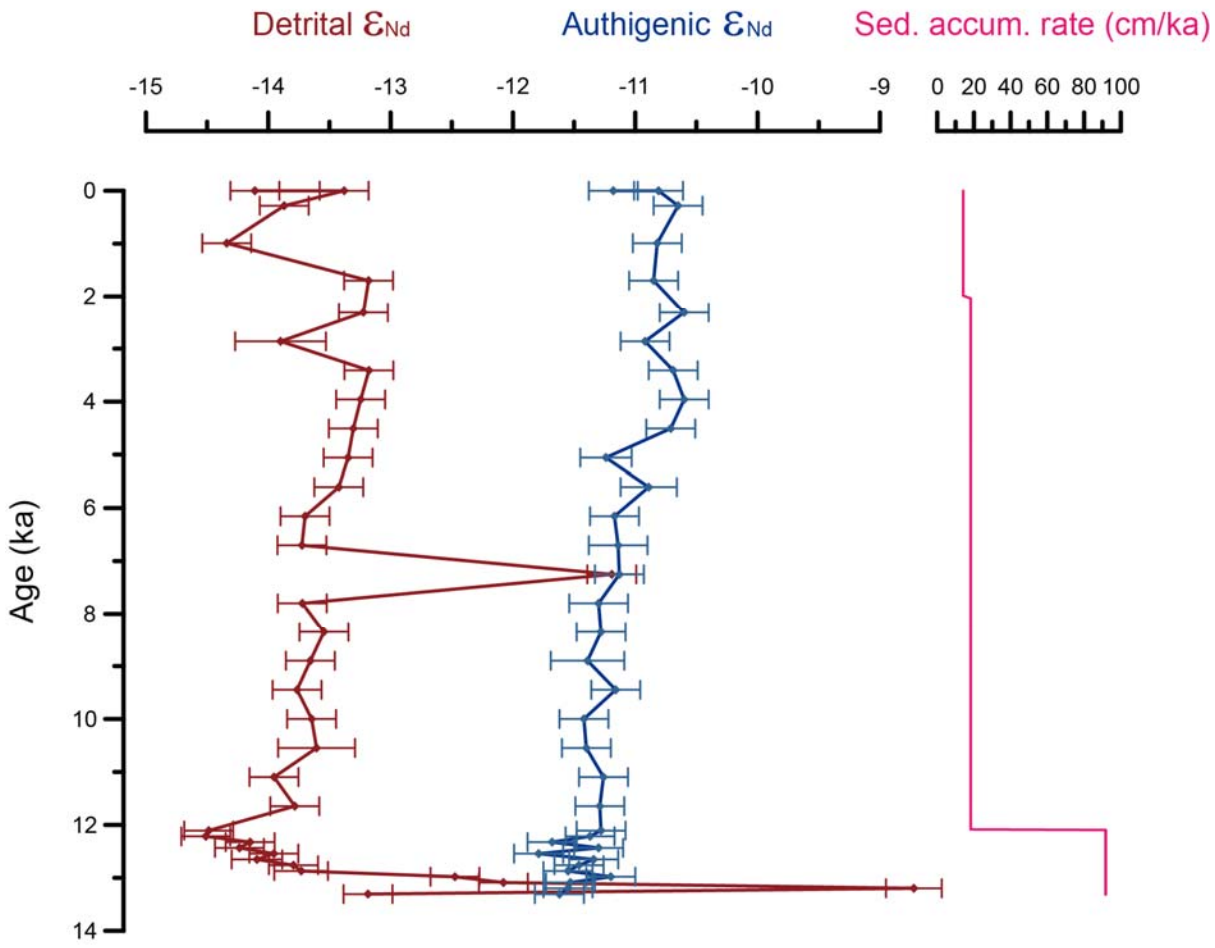

Figure 6. Temporal variation in ε_{Nd} values of detrital (red) and authigenic (blue) components at site HH12-964 in Woodfjorden. The ε_{Nd} data are compared to the sediment accumulation rate (Hansen, 2014). Error bars for ε_{Nd} represent ±2σ uncertainties.

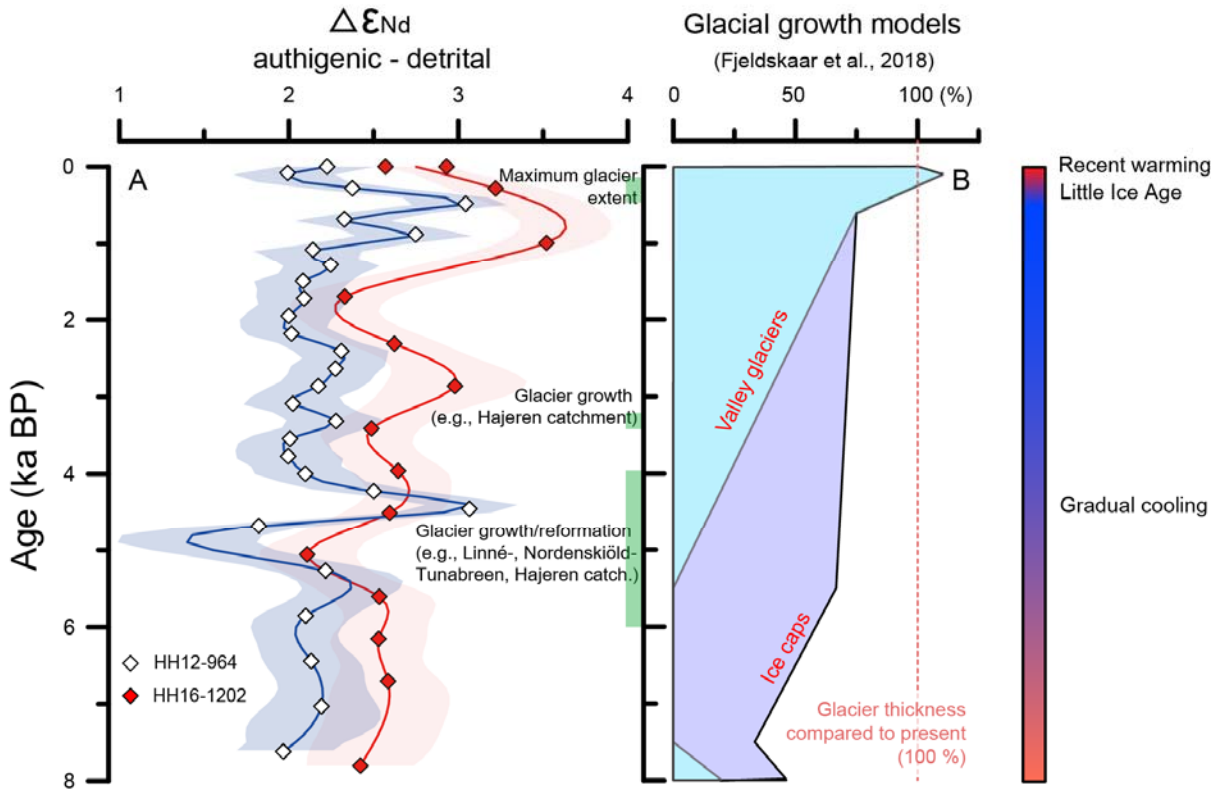

Figure 7. Comparison of (A) the differences between the authigenic and detrital ε_{Nd} values ($\triangle\varepsilon_{Nd}$) at core sites HH12-964 (red) and HH16-1202 (blue) and (B) the glacier thickness reconstructed by the best-fit model after Fjeldskaar et al. (2018) over the last 8 ka. Higher $\triangle\varepsilon_{Nd}$ values typically occur during the periods of glacier advances (green bars). Error ranges for $\triangle\varepsilon_{Nd}$ were calculated based on a smoothing spline Monte-Carlo simulation (2σ, resampled at every 0.1 ka, n = 100,000).

730 **Table 1.** Detrital and weatherable ε_{Nd} values of Svalbard bedrocks.

Sample ID	Coordinate	Area	Stratigraphic unit	Age*	Rock type	Detrital ε_{Nd}	Weatherable ε_{Nd}
13071104	78.987˚N, 12.087˚E	Blomstrandhalvøya, Kongsfjorden	Generalfjella Formation (Fm.), Krossfjorden Group	Upper Proterozoic	Quartzite	-8.8 ± 0.2	-5.8 ± 0.2
13071105	78.987˚N, 12.087˚E	Blomstrandhalvøya, Kongsfjorden	Generalfjella Fm., Krossfjorden Group	Upper Proterozoic	Phyllite	-11.7 ± 0.3	-11.4 ± 0.4
SK01	78.545˚N, 16.183˚E	Skansen, Isfjorden-Billefjorden	Wood Bay Fm., Dicksonfjorden Member	Devonian	Sandstone	-8.6 ± 0.3	-6.4 ± 0.3
080302	79.389˚N, 13.622˚E	Halvdanpiggen, Woodfjorden	Wood Bay Fm.	Devonian	Red sandstone	-13.6 ± 0.3	-10.8 ± 0.2
13071005	78.953˚N, 11.758˚E	Brøggerhalvøya, Kongsfjorden	Brøggertinden Fm.	Carboniferous	Red sandstone	-3.6 ± 1.3	-12.6 ± 0.2
SYB05	78.944˚N, 11.724˚E	Brøggerhalvøya, Kongsfjorden	Wordiekammen Fm.	Carboniferous	Limestone	-	-
SYB56	78.941˚N, 11.703˚E	Brøggerhalvøya, Kongsfjorden	Wordiekammen Fm.	Carboniferous	Dolostone	-	-10.9 ± 0.6
SK20	78.539˚N, 16.159˚E	Skansen, Isfjorden-Billefjorden	Wordiekammen Fm.	Carboniferous	Dolostone	-	-
SYB40.1	78.942˚N, 11.704˚E	Brøggerhalvøya, Kongsfjorden	Wordiekammen Fm.	Carboniferous - Permian	Calcareous shale	-16.3 ± 0.3	-13.7 ± 0.3
SF00.5	78.915˚N, 11.654˚E	Brøggerhalvøya, Kongsfjorden	Kapp Starotin Fm.	Permian	Chert	-11.6 ± 0.5	-6.6 ± 0.2
080109	78.091˚N, 13.81˚E	Festningen, Isfjorden-Grønfjorden	Kapp Starotin Fm.	Permian	Black mudstone	-8.5 ± 0.3	-6.8 ± 0.2
Sval central	78.545˚N, 16.183˚E	Skansen, Isfjorden-Billefjorden	Kapp Starotin Fm.	Permian	Anhydrite	-	-
KIGAM #25	78.475˚N, 15.812˚E	Rotundafjellet, Isfjorden-Billefjorden	Sassendalen Group	Early – Mid. Triassic	Shale	-6.1 ± 0.4	-9.3 ± 0.2
080111	78.094˚N, 13.837˚E	Festningen, Isfjorden-Grønfjorden	Verdebukta Fm.	Triassic	Black mudstone	-10.6 ± 0.3	-8.7 ± 0.2
20150901-02	78.341˚N, 15.857˚E	Janusfjellet, Isfjorden-Adventfjorden	Marhøgda Bed, Agardhfjellet Fm.	Jurassic	Oolitic ironstone	-6.3 ± 0.3	-5.1 ± 0.3
KIGAM #16	78.098˚N, 13.913˚E	Festningen, Isfjorden-Grønfjorden	Janusfjellet Subgroup	Mid. Jurassic - Early Cretaceous	Shale	3.4 ± 0.4	-1.2 ± 0.3
KIGAM #5	78.239˚N, 15.337˚E	Platåberget, Isfjorden-Adventfjorden	Carolinefjellet Fm.	Early Cretaceous	Shale	-9.0 ± 0.2	-12.0 ± 0.2
080114	78.099˚N, 13.948˚E	Festningen, Isfjorden-Grønfjorden	Helvetiafjellet Fm.	Cretaceous	Sandstone	-25.9 ± 0.2	-25.6 ± 0.2

731 *Dallmann and Elvevold (2015)